

TAMING GENERATIVE DIFFUSION PRIOR FOR UNIVERSAL BLIND IMAGE RESTORATION

A PREPRINT

Siwei Tu, Weidong Yang[†], Ben Fei[†]

Fudan University

24110240079@m.fudan.edu.cn, wdyang@fudan.edu.cn, bfei21@m.fudan.edu.cn

ABSTRACT

Diffusion models have been widely utilized for image restoration. However, previous blind image restoration methods still need to assume the type of degradation model while leaving the parameters to be optimized, limiting their real-world applications. Therefore, we aim to tame generative diffusion prior for universal blind image restoration dubbed **BIR-D**, which utilizes an **optimizable convolutional kernel** to simulate the degradation model and dynamically update the parameters of the kernel in the diffusion steps, enabling it to achieve blind image restoration results even in various complex situations. Besides, based on mathematical reasoning, we have provided an empirical formula for the chosen of **adaptive guidance scale**, eliminating the need for a grid search for the optimal parameter. Experimentally, Our BIR-D has demonstrated superior practicality and versatility than off-the-shelf unsupervised methods across various tasks both on real-world and synthetic datasets, qualitatively and quantitatively. BIR-D is able to fulfill multi-guidance blind image restoration. Moreover, BIR-D can also restore images that undergo multiple and complicated degradations, demonstrating the practical applications.

1 Introduction

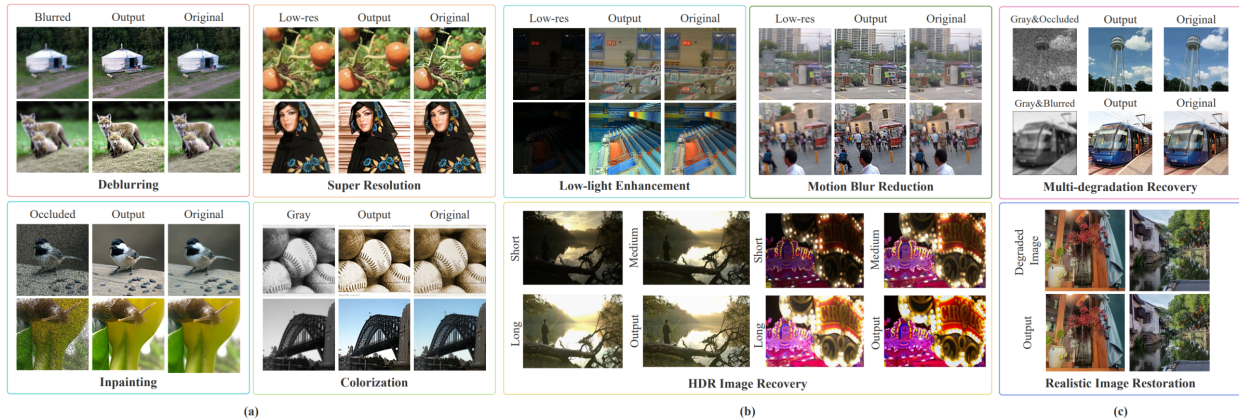


Figure 1: Blind Image Restoration Diffusion Model (BIR-D) can achieve high-quality restoration for different types of degraded images. BIR-D not only has the capability to restore (a) linear inverse problems when the degradation function is known. BIR-D can also achieve high-quality image restoration in (b) blind issues with unknown degradation functions, as well as in (c) mixed degradation and real degradation scenarios.

Images inevitably suffer from a degradation in quality in the process of capturing, storing, and compressing. Thus, the image restoration task intends to establish a mapping between the degraded image and the original image, to recover a high-quality image from the degraded image. In an ideal scenario, the ultimate goal is to undo and restore

the degradation process of the image. However, in reality, the complexity of the degradation mode often leads to the incapability to fully restore the original high-quality image, which also makes traditional supervised approaches unsuitable for all types of image restoration tasks. According to the degradation mode, image restoration tasks can be divided into two types: **non-blind** and **blind** problems. **Blind** problems, such as low light enhancement, motion blur reduction and HDR image restoration, refer to image restoration problems where the degradation functions and parameters are totally unknown.

The blind image restoration problem has attracted increasing attention with the development of generative models. The unsupervised blind image restoration methods represented by Generative Adversarial Networks (GANs) [1; 2; 3; 4] have the capability to train networks on large datasets of clean images and learn real-world knowledge. However, GANs are still difficult to avoid falling into limitations such as poor diversity and difficulty in model training. In parallel, diffusion model [5; 6; 7; 8; 9] have shown strong performance in terms of quality and diversity compared to GANs. Pioneer works such as GDP [10], DDRM [11], and DDNM [12] attempt to solve such problems by incorporating the degraded image y as guidance in the sampling process of diffusion models. By modeling posterior distributions in an unsupervised sampling manner, these approaches showcase the potential for practical guidance in blind image restoration, offering promising implications for real-world applications. However, the degradation types in these models still need to be assumed, limiting the practicality of natural image restoration where the complicated degradation models always remain unknown.

To this end, we propose an effective and versatile Blind Image Restoration Diffusion Model (BIR-D). It utilizes well-trained DDPM [13] as an effective prior and is guided by degraded images to form a universal method for various image restoration and enhancement tasks. To uniformly model the unknown degradation function of blind image restoration, an optimizable convolutional kernel is dynamically optimized and utilized to simulate the degradation function at each denoising step. Specifically, BIR-D updates the convolution kernel parameters based on the gradient of distance loss between the generated image undergoing our optimizable convolutional kernel and the given degraded image. At the same time, all existing image restoration methods [10; 11; 12] that use conditional diffusion models manually set the guidance scale as a hyperparameter to control the magnitude of guided generation, which also remains unchanged throughout the sampling process. However, for images from different tasks, the guidance scale required for each diffusion step is not entirely the same. To deal with this issue, we have derived an empirical formula for the guidance scale, which can calculate the optimal guidance scale for the next denoising step in real-time during the sampling process. This improvement avoids the need to manually grid search the optimal value of the guidance scale when solving different tasks and also enhances the quality of generated images. With the help of a well-trained DDPM, the above designs enable BIR-D to tackle various blind image restoration tasks. BIR-D can also achieve multi-degradation or multi-guidance image restoration. Furthermore, it showcases satisfactory results in addressing restoration issues related to complex degradation types encountered in real-world scenarios.

2 Related Work

Diffusion Model for Image Restoration. Image restoration and denoising have seen various advancements with diffusion-based models [14; 15]. They have been thoroughly explored for linear inverse problems [11; 10], nonlinear inverse problems [16; 10]. To alleviate the fixed- and small-size generation of diffusion models, patch-based algorithm [17] and large-size generation [18; 12] are proposed. Our model introduces the guidance of degraded images to form an unconditional diffusion model, and attempts to simulate and update the degradation function in real-time, making it suitable for general tasks while maintaining both image quality and efficiency.

Blind Image Restoration. Many problem-solving approaches have emerged in the field of blind image restoration [19]. The emergence of GANs [2; 20] provides several solutions for unsupervised learning in blind image restoration. On top of GANs, DDPMs are more studied for this task due to the enhanced diversity. For instance, both DiffBIR [15] and GDP [10] leverage generative diffusion priors for blind image restoration. BlindDPS [21] introduces parallel diffusion models for solving blind inverse problems when the functional forms are known. PromptIR [22] uses prompts to encode degradation-specific information and dynamically guide the recovery of the network. Nevertheless, these methods are still limited to specific tasks. BIR-D can be regarded as a unified solver for multiple restoration tasks by simultaneously estimating the recovered images and specific degradation models.

3 Preliminary

Diffusion models consists of the forward and reverse processes. The forward process continuously adds noise to a natural image x_0 through T diffusion steps to obtain the noise distribution $x_T \sim \mathcal{N}(0, I)$, where \mathcal{N} represents the

Gaussian distribution. The reverse process aims to simulate the noise in each diffusion step and eliminate it, ultimately obtaining the restored generated image x_0 .

The forward process is a Markov chain defined by the following equation:

$$q(x_1, \dots, x_T | x_0) = \prod_{t=1}^T q(x_t | x_{t-1}) \quad (1)$$

It corrupts the initial data x_0 into distribution x_T that is close to Gaussian noise after T steps of diffusion, with each sample process defined by $q(x_t | x_{t-1}) = \mathcal{N}(x_t; \sqrt{1 - \beta_t}x_{t-1}, \beta_t I)$, where β_t is the variance of a forward process. The variance can be set as a constant or learned by reparameterization. Simultaneously defining $\alpha_t = 1 - \beta_t, \bar{\alpha}_t = \prod_{i=1}^t \alpha_i$. It has been proven by [23] that through mathematical reasoning, x_t at any diffusion step can be directly calculated from the starting x_0 :

$$x_t = \sqrt{\bar{\alpha}_t}x_0 + \sqrt{1 - \bar{\alpha}_t}\epsilon, \quad (2)$$

where $\epsilon \sim \mathcal{N}(0, I)$. When T is large enough, $\sqrt{\bar{\alpha}_t}$ approaches 0, and at this point $q(x_T | x_0)$ is closer to the latent distribution of x_T .

The reverse process is also a Markov chain, which gradually denoises a standard multivariate Gaussian distribution into a denoised image x_0 . Firstly, sample $x_t \sim \mathcal{N}(0, I)$. The conditional distribution of the reverse process is $p_\theta(x_{t-1} | x_t) = \mathcal{N}(x_{t-1}; \mu_\theta(x_t, t), \Sigma_\theta I)$. According to the Bayesian formula, it can be transformed as follows:

$$q(x_{t-1} | x_t, x_0) = q(x_t | x_{t-1}, x_0) \frac{q(x_{t-1} | x_0)}{q(x_t | x_0)} \quad (3)$$

Expand and simplify the three terms at the right end of the equation. The variance Σ_θ of the reverse process can be obtained as a fixed value. Note that [24] indicates that it can also be learned parameters. And the mean of the reverse process μ_θ related to x_t and \tilde{x}_0 :

$$\tilde{\mu}_t(x_t, \tilde{x}_0) = \frac{\sqrt{\bar{\alpha}_t - 1}\beta_t}{1 - \bar{\alpha}_t}\tilde{x}_0 + \frac{\bar{\alpha}_t(1 - \bar{\alpha}_{t-1})}{1 - \bar{\alpha}_t}x_t \quad (4)$$

According to the formula of the forward process, \tilde{x}_0 can be predicted by x_t , where ϵ is a noise function approximator obtained by a neural network θ .

$$\tilde{x}_0 = \frac{x_t}{\sqrt{\bar{\alpha}_t}} - \frac{\sqrt{1 - \bar{\alpha}_t}\epsilon_\theta(x_t, t)}{\sqrt{\bar{\alpha}_t}} \quad (5)$$

Substitute it into eq. (4) to obtain the mean value μ_θ :

$$\mu_\theta(x_t, t) = \frac{1}{\sqrt{\bar{\alpha}_t}}\left(x_t - \frac{\beta_t}{\sqrt{1 - \bar{\alpha}_t}}\epsilon_\theta(x_t, t)\right) \quad (6)$$

4 BIR-D: Universal Blind Image Restoration Diffusion Model

In this study, we aim to use a well-trained DDPM [13] to learn the prior distribution of images and ultimately solve non-blind and blind problems in various image restoration tasks.

4.1 Optimizable convolutional kernel as a universal degradation function

For a natural image x , its corresponding degraded image y can be obtained by the degradation function $y = \mathcal{D}(x)$. Most of the blind image restoration methods [10; 12] are used to solve the situation where the degradation function \mathcal{D} is known while leaving the parameters of \mathcal{D} are unknown. However, when dealing with real-world image restoration problems, the degradation function \mathcal{D} is not only an unknown quantity but also difficult to accurately represent mathematically. Therefore, we propose an optimized convolutional kernel to simulate complex degradation functions. The parameters of the convolution kernel in the degradation function are dynamically optimized along with the denoising steps.

Moreover, in the real-world scenario, considering that there are different noises in different subtle areas of the image, using only one optimized convolutional kernel may not fully cover this situation. Therefore, we propose to utilize a mask \mathcal{M} to model and estimate these noises. Thus, the entire degradation process can be represented as: $y = \mathcal{K}(x) + \mathcal{M}$, where \mathcal{K} refers to the optimized convolutional kernel used in the model and \mathcal{M} is a mask with the same dimension as image x . \mathcal{K} and \mathcal{M} have their own optimizable parameters, forming the degradation function *mathcal{D}*. In this way, any degradation process can be simulated by this degradation function.

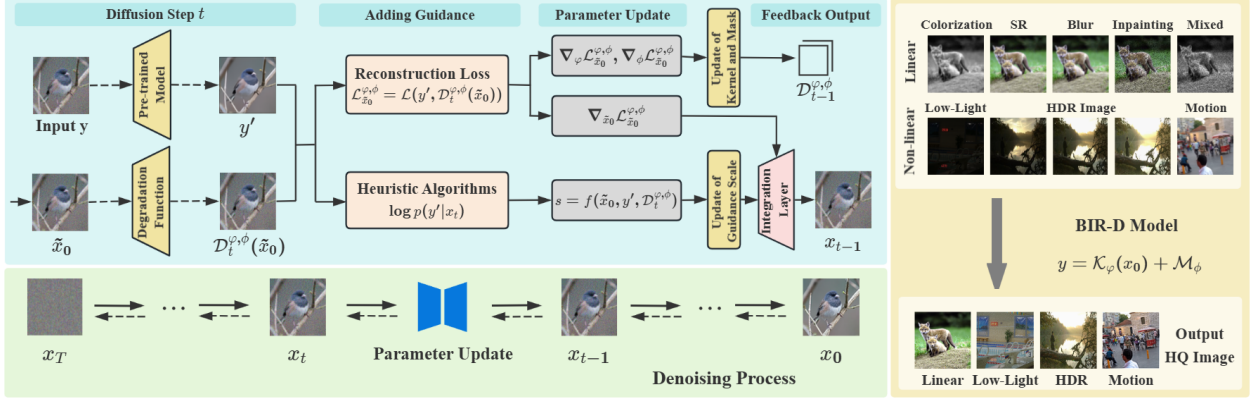


Figure 2: **Overview of BIR-D.** Degraded image y was given during the sampling process. BIR-D systematically incorporates guidance from degraded images in the reverse process of the diffusion model and optimizes the degraded model at the same time. For degraded image y , pre-training is first performed to provide a better initial state for BIR-D. BIR-D introduces a distance function in each step of the reverse process of the diffusion model to describe the distance loss between the degraded image y and the generated image \tilde{x}_0 after the degradation function, so that the gradient could be used to update and simulate a better degradation function. Based on the empirical formula, the adaptive guidance scale can be calculated to provide optimal guidance during the sampling process.

4.2 Empirical formula of guidance scale

In the reverse denoising process of DDPM, the generated images can be conditioned on degraded image y [48]. Specifically, the distribution $p_{\theta}(x_{t-1}|x_t)$ of reverse denoising is converted into a conditional distribution $p_{\theta}(x_{t-1}|x_t, y)$. It is demonstrated [13] that the difference between it and the original formula lies in the addition distribution of $p(y|x_t)$, which serves as a probability representation for denoising x_t into a high-quality image consistent with y . Previous work [10] proposed a feasible calculation to approximate this indicator by using heuristic algorithms:

$$\log p(y | x_t) = -\log N - s\mathcal{L}(\mathcal{D}(\tilde{x}_0), y), \quad (7)$$

where N is the normalization factor, which is the distribution $p_{\theta}(y|x_{t+1})$, and s is the scalar factor used to control the importance of guidance, named guidance scale. \mathcal{L} is the distance metric.

The value of the guidance scale plays a crucial role in the quality of the image generation result. A larger value can lead to overall blurring of the image, while a smaller value can result in missing details in the restoration. However, the guidance scale in existing works [10; 9; 12] can only be manually set as a hyperparameter. But in specific experiments,

Algorithm 1: Conditional diffusion model with the guidance of degraded image y , given a diffusion model noise prediction function $\epsilon_{\theta}(x_t, t)$.

Input: Degraded image y , degradation function \mathcal{D} composed of optimized convolutional kernels \mathcal{K} with parameters φ and mask \mathcal{M} with parameters ϕ , learning rate l , distant measure \mathcal{L} .

Output: Output image x_0 conditioned on y .

Sample x_T from $\mathcal{N}(0, I)$

for t from T to 1 **do**

$$\begin{aligned} \tilde{x}_0 &= \frac{x_t}{\sqrt{\alpha_t}} - \frac{\sqrt{1-\alpha_t}\epsilon_{\theta}(x_t, t)}{\sqrt{\alpha_t}} \\ \mathcal{L}_{\varphi, \phi, \tilde{x}_0} &= \mathcal{L}(y, \mathcal{D}^{\varphi, \phi}(\tilde{x}_0)) \\ s &= -\frac{(x_t - \mu)^T g + C + \log N}{\mathcal{L}(\mathcal{D}^{\varphi, \phi}(\tilde{x}_0), y)} \\ \tilde{x}_0 &\leftarrow \tilde{x}_0 - \frac{s(1-\alpha_t)}{\sqrt{\alpha_{t-1}\beta_t}} \nabla_{\tilde{x}_0} \mathcal{L}_{\varphi, \phi, \tilde{x}_0} \\ \tilde{\mu}_t &= \frac{\sqrt{\alpha_{t-1}\beta_t}}{1-\alpha_t} \tilde{x}_0 + \frac{\sqrt{\alpha_t(1-\alpha_{t-1})}}{1-\alpha_t} x_t \\ \tilde{\beta}_t &= \frac{1-\alpha_{t-1}}{1-\alpha_t} \beta_t \\ \text{Sample } x_{t-1} &\text{ from } \mathcal{N}(\tilde{\mu}_t, \tilde{\beta}_t I) \\ \varphi &\leftarrow \varphi - l \nabla_{\varphi} \mathcal{L}_{\varphi, \phi, \tilde{x}_0} \\ \phi &\leftarrow \phi - l \nabla_{\phi} \mathcal{L}_{\varphi, \phi, \tilde{x}_0} \end{aligned}$$

return x_0



Figure 3: Comparison of image quality for blind face restoration results on LFW [25] and WIDER dataset [26].

Task	LFW dataset		WIDER dataset	
	FID	NIQE	FID	NIQE
PGDiff [14]	71.62	4.15	39.17	3.93
DiffBIR [15]	39.58	4.03	32.35	3.78
BIR-D	40.12	3.94	31.49	3.65

Table 1: Quantitative comparison of blind face restoration on LFW and WIDER datasets

the optimal value of the guidance scale varies in different masks, degraded images, and diffusion steps. The original configuration necessitates thorough testing for the initial setup. Additionally, employing the same guidance scale for every denoising step is not an optimal choice.

Therefore, we propose an empirical formula for the guidance scale, which can dynamically calculate and update the optimal values of guidance factors in real-time at each diffusion step of degraded images in specific repair tasks. Specifically, we noticed that the distribution $\log p_{\theta}(y|x_t)$ can be applied to perform Taylor expansion around $x = \mu$ and take the first two terms.

$$\log p_{\theta}(y | x_t) \approx \log p(y | x_t) |_{x_t=\mu} + (x_t - \mu)^T \nabla_{x_t} \log p_{\theta}(y | x_t) |_{x_t=\mu} \quad (8)$$

$$= (x_t - \mu)^T g + C, \quad (9)$$

where $g = \nabla_{x_t} \log p_{\theta}(y | x_t) |_{x_t=\mu}$, $C = \log p(y | x_t) |_{x_t=\mu}$. By combining the heuristic approximation formula and Taylor expansion formula mentioned above, we can simplify the empirical formula for the guidance scale:

$$s = -\frac{(x_t - \mu)^T g + C + \log N}{\mathcal{L}(\mathcal{D}(x_t), y)} \quad (10)$$

For each image at every moment t , the applicable value of the guidance scale can be calculated. However, because y is a degraded image without noise, while x_t itself has noise. The use of MSE loss between x_t and y can lead to the introduction of noise into the guidance process. Therefore, we utilize the MSE error between the estimated value \hat{x}_0 and y here, and the above formula could be corrected as:

Task	4×Super resolution				Deblur				25% Inpainting				Colorization			
	PSNR	SSIM	Consistency	FID	PSNR	SSIM	Consistency	FID	PSNR	SSIM	Consistency	FID	PSNR	SSIM	Consistency	FID
RED[28]	24.18	0.71	27.57	98.30	21.30	0.58	63.20	69.55	-	-	-	-	-	-	-	-
DGP[27]	21.65	0.56	158.74	152.85	26.00	0.54	475.10	136.53	27.59	0.82	414.60	60.65	18.42	0.71	305.59	94.59
SNIPS[29]	22.38	0.66	21.38	154.43	24.73	0.69	60.11	17.11	17.55	0.74	587.90	103.50	-	-	-	-
DDRM[11]	26.53	0.78	19.39	40.75	35.64	0.98	50.24	4.78	34.28	0.95	4.08	24.09	22.12	0.91	37.33	47.05
DDNM[30]	25.36	0.81	7.52	39.14	24.66	0.71	41.70	4.64	32.16	0.96	5.42	17.63	21.95	0.89	36.41	38.79
GDP[10]	24.42	0.68	6.49	38.24	25.98	0.75	41.27	2.44	34.40	0.96	5.29	16.58	21.41	0.92	36.92	37.60
BIR-D	24.58	0.71	6.32	37.54	26.31	0.73	38.42	2.32	33.59	0.90	5.18	15.73	22.09	0.89	36.12	36.58

Table 2: Quantitative comparison of linear inverse problems on ImageNet 1k[27].

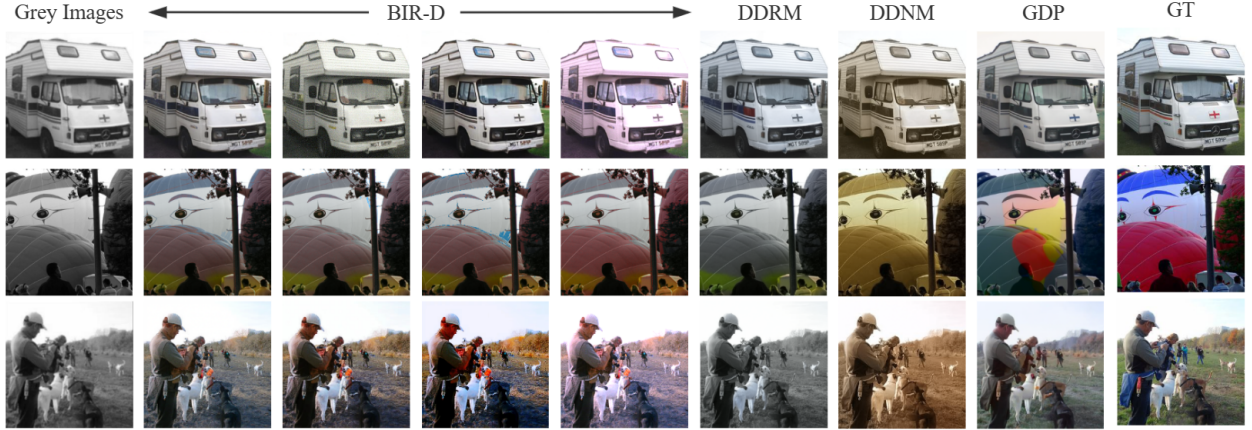


Figure 4: Comparison of colorization image on ImageNet 1k[27]. BIR-D can generate various outputs on the same input image.

$$s = -\frac{(x_t - \mu)^T g + C + \log N}{\mathcal{L}(\mathcal{D}(\tilde{x}_0), y)}. \quad (11)$$

The guidance scale is related to the generated images x , degraded image y , and the degradation function \mathcal{D} . This value of this **Adaptive Guidance Scale** can be dynamically updated in each diffusion step so that each step in the diffusion model can use the most appropriate guidance scale.

4.3 Sampling process of BIR-D

Through empirical formulas, we can obtain the conditional transition formula in the reverse process of the diffusion model.

$$\log p_\theta(x_t|x_{t+1}, y) = \log(p_\theta(x_t|x_{t+1})p(y|x_t)) + N_1 \quad (12)$$

$$\approx \log p(z) + N_2, \quad (13)$$

where z conforms to the distribution $\mathcal{N}(z; \mu_\theta(x_t, t) + \Sigma g, \Sigma)$. The intermediate quantity $g = \nabla_{x_t} \log p(y|x_t)$. The value of g can be obtained by calculating the gradient in heuristic algorithms in eq. (7), which includes the parameter of guidance scale:

$$g = \nabla_{x_t} \log p(y|x_t) = -s \nabla_{x_t} \mathcal{L}(\mathcal{D}(x_t), y) \quad (14)$$

The other terms N_1 , N_2 , and the variance of the reverse process $\Sigma = \Sigma_\theta(x_t)$ in eq. (12) and eq. (13) are constants, and the unconditional distribution $p_\theta(x_{t-1}|x_t)$ is given by traditional diffusion models.

Therefore, the conditional transition distribution $p(x_{t-1}|x_t, y)$ can be approximately estimated by adding $-(s \Sigma \nabla_{x_t} \mathcal{L}(\mathcal{D}(x_t), y))$ to the mean of the traditional unconditional transition distribution. Previous studies [10] have shown that the addition of Σ has a negative impact on the quality of generated images. Therefore, in this experiment, we omitted the term Σ , and the complete sampling process is shown in algorithm 1.

Detailly, in the diffusion step t of the sampling process, the noise of x_t is first predicted from the given pre-trained DDPM and eliminated to obtain an estimated value of x_0 . Subsequently, apply the degradation function of step t to x_0

Figure 5: Results of linear degradation tasks on 256×256 images from ImageNet 1k.

Task	LOL					VE-LOL-L				
	PSNR	SSIM	LOE	FID	PI	PSNR	SSIM	LOE	FID	PI
ExCNet[34]	16.04	0.62	220.38	111.18	8.70	16.20	0.66	225.15	115.24	8.62
Zero-DCE[35]	14.91	0.70	245.54	81.11	8.84	17.84	0.73	194.10	85.72	8.12
Zero-DCE++[36]	14.86	0.62	302.06	86.22	7.08	16.12	0.45	313.50	86.96	7.92
RRDNet[37]	11.37	0.53	127.22	89.09	8.17	13.99	0.58	94.23	83.41	7.36
GDP[10]	13.93	0.63	110.39	75.16	6.47	13.04	0.55	79.08	78.74	6.47
BIR-D	14.52	0.56	105.42	68.98	4.87	13.87	0.51	78.18	74.54	5.73

Table 3: Quantitative comparison among various zero-shot learning methods of low-light enhancement task on LOL [31] and VE-LOL-L [32] Bold font represents the best metric result.

and calculate its reconstruction loss with the degraded image y . We utilize our adaptive guidance scale for sampling the next step latent x_{t-1} . In this process, it is necessary to calculate the gradient about x_0 and the parameters of each convolution kernel in the distance metric loss, which is used to update the convolution kernel parameters in real time for the next sampling process.

Pre-process. The empirical formula for the guidance scale we construct is related to the degradation function. Herein, when the model simulates the degradation function more reasonably, BIR-D can obtain more appropriate guidance scale values accordingly. To this end, we introduce a first-stage pre-training model from [15] to further enhance the model’s capability to correct initial deviations. This enables the model to have a strong correction ability for significant deviations in the degradation function during the initial diffusion step, ultimately generating ideal image restoration results.

Multi-degradation Image Restoration. In the real world, the degradation process often involves a combination of multiple different complex types. To improve the image restoration capability of the model in complex situations and enhance its practicality, we propose to extend BIR-D into multi-task scenarios. To our surprise, BIR-D can fulfill multi-degradation image restoration without any modification (Figure 9) thanks to the mixture of degradation types can also be simulated as an unknown degradation by an optimizable convolutional kernel.

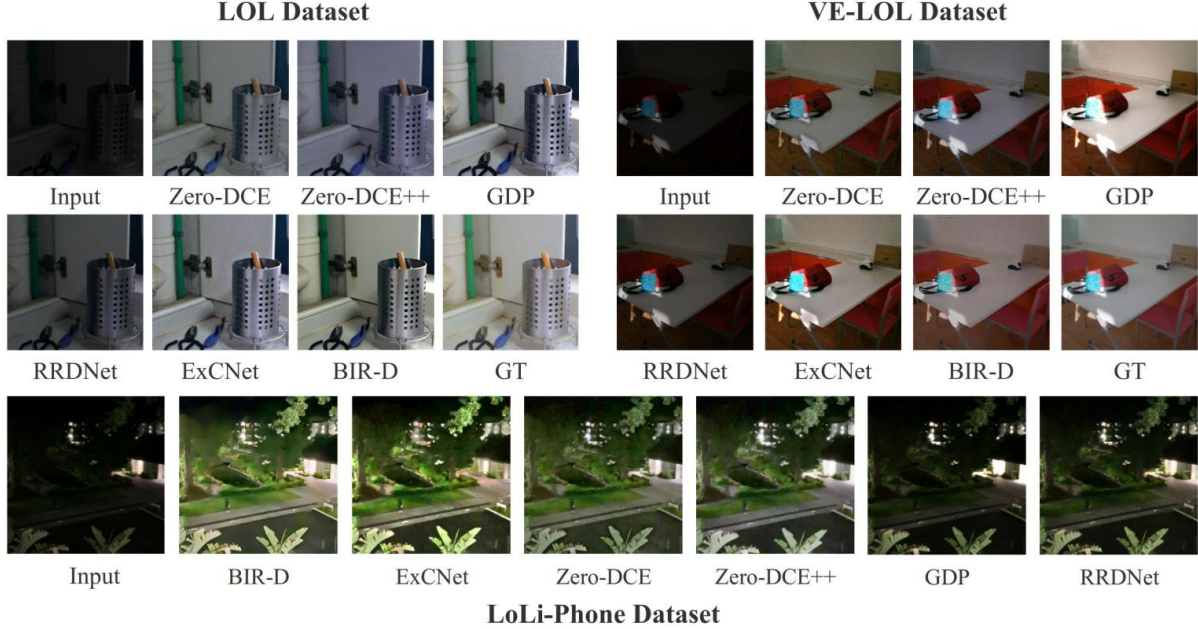


Figure 6: Comparison of image quality in low-light enhancement task on the LoL [31], VE-LoL [32] and LoLi-Phone [33] datasets.



Figure 7: Comparison of image quality for HDR image recovery results on NTIRE [38].

5 Experiments

In this section, we systematically compare BIR-D with other blind image restoration methods in real-world and synthetic datasets.

Blind Image Restoration on Real-world Datasets. Firstly, we evaluate the blind image restoration capability of BIR-D on two real-world datasets, namely LFW dataset [25] and WIDER dataset [26]. As shown in Figure 3, BIR-D successfully simulated and removed blur, and achieved more ideal facial detail restoration. The quantitative results in Table 1 shows that BIR-D outperforms PGDiff [14] and DiffBIR [15] in NIQE metric on both datasets and FID metric on WIDER, demonstrating better blind image restoration performance.

Comparison on Common Linear Inverse Problems. We conducted experiments on linear inverse problems on ImageNet 1k to compare BIR-D with off-the-shelf methods. For each experiment, we calculated the average Peak Signal-to-Noise Ratio (PSNR), Structural Similarity (SSIM), Consistency, and FID results, where PSNR, SSIM, and Consistency are used to quantify the faithfulness between the generated image and the original image, while FID is used to measure the quality of the generated image. To make fair comparisons, other methods are given known degradation functions as reported in the original paper while BIR-D utilizes universal degradation functions for different tasks. Table 2 shows that BIR-D outperforms other methods in terms of Consistency and FID in almost all tasks. As shown in Figure 5, the images generated by BIR-D demonstrate a high level of image quality and details. Moreover, Figure 4 also demonstrates that BIR-D can generate various results in image restoration tasks.

Low Light Enhancement. We further evaluated the effectiveness of BIR-D in low-light image enhancement. Following the previous works [10], we utilized three datasets, LOL [31], VE-LoL-L [32], and LoLi-Phone [33], to test the restoration ability of BIR-D. As shown in Table 3, our BIR-D outperforms all the zero-shot methods in both FID and Lightness Order Error (LOE) [49], and demonstrates significant improvement in Perceptual index (PI) [50]. A lower PI value reflects better perceptual quality, while a lower LOE reflects a better natural preservation ability of the generated

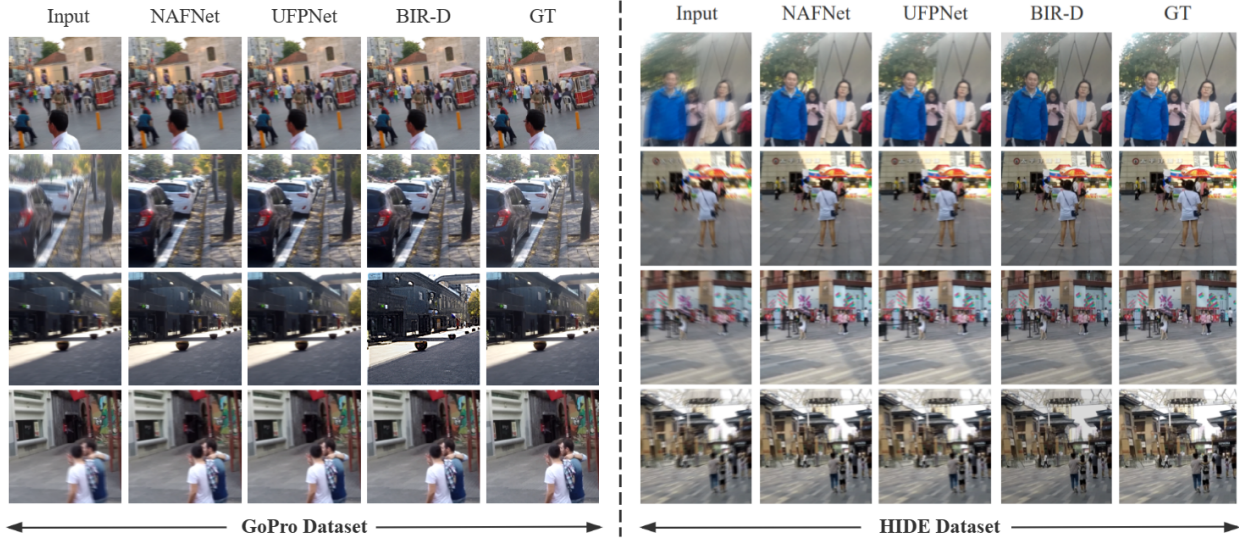


Figure 8: Comparison of image quality for motion blur reduction results on GoPro [39] and HIDE dataset [40].

Motion Blur Reduction	GoPro		HIDE		HDR Recovery	NTIRE			
	PSNR	SSIM	PSNR	SSIM		PSNR	SSIM	LPIPS	FID
DeepRFT[41]	33.23	0.963	31.42	0.944	Deep-HDR[42]	21.66	0.76	0.26	57.52
MSDI-Net[43]	33.28	0.964	31.02	0.940	AHDRNet[44]	18.72	0.58	0.39	81.98
NAFNet[45]	33.69	0.967	31.32	0.943	HDR-GAN[46]	21.67	0.74	0.26	52.71
UFPNet[47]	34.06	0.968	31.74	0.947	GDP[10]	24.88	0.86	0.13	50.05
BIR-D	34.12	0.968	32.09	0.948	BIR-D	25.03	0.88	0.16	48.74

Table 4: Quantitative comparison of motion blur reduction and HDR image recovery tasks.

image, making images to have a more natural sensory experience. As shown in Figure 6, BIR-D exhibits reasonable and well-exposed results.

HDR Image Recovery. In the HDR image restoration task, we compared BIR-D with other leading methods, including DeepHDR [42], AHDRNet [44], HDR-GAN [46], and GDP [10], on the NTIRE2021 Multi-Frame HDR Challenge [38] dataset. The quantitative and qualitative results are presented in Table 4 and Figure 7, with BIR-D showing the best PSNR and SSIM levels, and successfully generating results with rich and accurate detailed information.

Motion Blur Reduction. To evaluate the performance of BIR-D in the motion blur reduction tasks, we compare BIR-D with the state-of-the-art motion blur reduction methods on GoPro dataset [39] and HIDE dataset [40]. We used the same input image, which also means that the motion blur of the input image is the same, ensuring fairness in comparison. The comparison results of the metrics are presented in Table 4, where BIR-D outperforms existing methods in both PSNR and SSIM. As shown in Figure 8, BIR-D can effectively achieve the elimination of motion blur. The generated images not only achieve a better quality but also receive restoration with more clear details.

Multi-Degradation Image Restoration. Encouraged by the excellent restoration performance of BIR-D on single restoration task, we further tested the image restoration performance of BIR-D in solving multi-task image restoration. As shown in Figure 9, we take a degraded image on the ImageNet dataset where two types of degradation are mixed as

Methods	Dynamic Update		LOL					LoLi-Phone	
	Kernel	Guidance Scale	PSNR	SSIM	LOE	FID	PI	LOE	PI
Model A	✗	✗	8.96	0.46	210.88	113.36	8.24	110.05	8.36
Model B	✗	✓	9.58	0.48	203.83	102.47	7.90	102.55	8.25
Model C	✓	✗	14.35	0.54	113.56	82.14	5.23	75.34	7.94
BIR-D	✓	✓	14.52	0.56	105.42	68.98	4.87	72.83	6.12

Table 5: The ablation study on the optimizable convolutional kernel and the empirical settings of guidance scale.

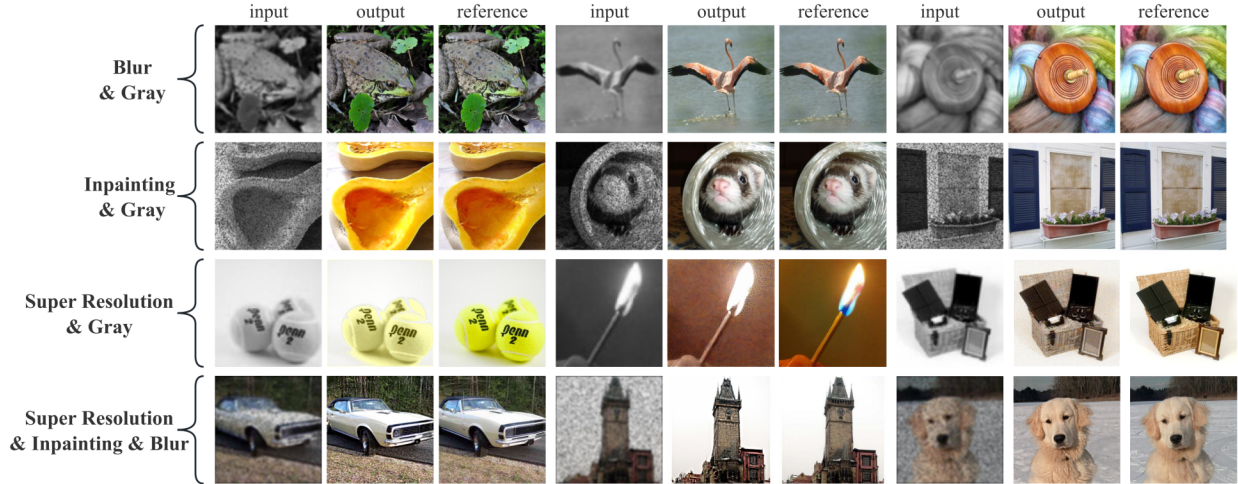


Figure 9: Results of multi-task image restoration.

Task	Low-Light Enhancement					Motion Blur Reduction	
	PSNR	SSIM	LOE	FID	PI	PSNR	SSIM
kernel size=1	13.73	0.49	118.38	78.52	5.67	31.14	0.917
kernel size=3	13.90	0.54	113.89	74.41	5.24	32.07	0.937
kernel size=7	14.47	0.56	108.75	70.55	4.93	33.94	0.961
BIR-D with 5×5 kernel	14.52	0.56	105.42	68.98	4.87	34.12	0.968

Table 6: The ablation study of kernel size in blind issues.

an example. The optimizable convolution kernel of BIR-D can also simulate these complicated degradation functions. The generated images obtained have excellent results in both image quality and details.

5.1 Ablation study

The Effectiveness of Optimizable Convolutional Kernel and Adaptive Guidance Scale. The ablation studies on the real-time optimizable convolutional kernel parameters and guidance scale were performed to reveal the effectiveness of these settings. We further tested the LOL [31] and the most challenging LoLi-phone [33] datasets. Model A fixed the convolutional kernel parameters and guidance scale. Models B and C represent fixed parameters for the convolution kernel and the fixed guidance scale, respectively. As shown in Table 5, BIR-D outperformed other models in all indicators, demonstrating the effectiveness of an optimizable convolutional kernel and adaptive guidance scale.

The Optimal Size of Optimizable Convolutional Kernel. In the main paper, in order to assure the versatility of BIR-D, we used convolution kernels of size 7×7 for all tasks. Nevertheless, for different types of tasks, the size of the convolution kernel might be different. To explore the impact of kernel size on the quality of generated images, we conducted experiments using convolution kernels of different sizes in various types of image restoration tasks. As shown in Table 6, for blind image restoration tasks, the experiment showed that the results of a 5×5 convolution kernel perform best. For linear inverse tasks (Table 7), the optimal convolution kernel size was 9×9 .

The Effectiveness of the First Stage Pre-training Model. We conducted further experiments on the deblur task to demonstrate the impact of the first-stage pre-training model. As shown in Table 8, for a randomly initialized convolution kernel parameter, all metrics of BIR-D were better than BIR-D without the pre-training model. These results indicate that the first-stage pre-trained model is able to provide better initial state of images for our BIR-D.

6 Parameter analysis

The Parameter Variations of the Optimizable Convolution Kernel and Mask in the Reverse Steps. In order to visualize the variation trends of the parameters of convolution kernel mask in the reverse process, we conducted experiments on the test set of the LOL dataset from the low-light enhancement task. As shown in Figure 11(a), the mean

Task	4 × Super resolution				Deblur			
	PSNR	SSIM	Consistency	FID	PSNR	SSIM	Consistency	FID
kernel size=13	24.05	0.66	6.65	39.02	26.12	0.74	41.29	3.09
kernel size=7	24.31	0.67	6.64	38.91	26.53	0.77	38.60	2.53
kernel size=11	24.36	0.69	6.50	38.07	26.79	0.79	38.52	2.44
BIR-D with 9 × 9 kernel	24.58	0.71	6.32	37.54	27.14	0.84	37.86	2.32
Task	25% Inpainting				Colorization			
	PSNR	SSIM	Consistency	FID	PSNR	SSIM	Consistency	FID
kernel size=7	29.58	0.80	6.17	18.09	20.07	0.76	39.85	42.29
kernel size=13	31.12	0.84	5.64	16.56	21.04	0.83	37.71	38.14
kernel size=11	32.91	0.86	5.41	16.17	21.57	0.85	37.69	38.01
BIR-D with 9 × 9 kernel	33.59	0.90	5.18	15.73	22.09	0.89	36.12	36.58

Table 7: The ablation study of kernel size in linear inverse problem.

Task	Random initial value				Biased initial value			
	PSNR	SSIM	Consistency	FID	PSNR	SSIM	Consistency	FID
BIR-D without pre-training model	25.88	0.69	40.24	2.55	21.49	0.61	53.78	4.32
BIR-D	26.31	0.73	38.42	2.32	25.97	0.71	39.87	2.41

Table 8: The ablation study on the effectiveness of the pre-training model.

values of the convolution kernel parameters and degradation mask are given by random initialization and gradually increase with the progress of the time steps. This increase in magnitude is influenced by the gradient of the distance metric with respect to the corresponding parameters. When the sampling step $t < 500$, the difference between \tilde{x}_0 and y changes slightly, resulting in correspondingly smaller gradient values.

BIR-D employs masks in the degradation function with the intent to address the image restoration of local regions characterized by substantial shifts in brightness. Figure 11(b) shows that the mask \mathcal{M} of the degradation model has an upward trend from their initial values, making the overall degradation function approach the true degradation. As shown in Figure 12, during the sampling process, the degradation mask learns the detailed information of the image, including local regions with significant brightness differences. This process is obtained by updating the gradient of the distance metric with respect to the degradation mask parameters.

The Theoretical Analysis of the Changing Trend of Guidance Scale in the Reverse Steps. We take the variation in the guidance scale of BIR-D on the LOL dataset as an example to analyze the trend of its changes during the reverse steps. As shown in Figure 11(c), the guidance scale gradually decreases with the sampling step, which aligns with the actual situation. When the sampling step $t < 500$, as t decreases, the difference between x_t and x_{t-1} decreases with decreasing t , indicating a reduction in the simulated noise at each step. Therefore, the level of guidance required for each sampling step should also be reduced accordingly, leading to a decrease in the required guidance scale values. According to Equation (10), when step t is small, the gradient term g also decreases due to the small change in x_t at each step. The speed of the gradient term decreases is greater than the speed of distance metric decreases, resulting in a decrease in the value of the guidance scale.

7 Conclusion

In this paper, we propose Blind Image Restoration Diffusion, which is a unified model that can be used to solve various blind image restoration problems. We utilize optimized convolutional kernels to simulate and update the degradation function in the diffusion step in real time, and derive the empirical formula of the guidance scale in detail, so that it can better utilize the conditional diffusion model to generate high-quality images. The ability to solve various blind image restoration tasks, including low-light enhancement and motion blur reduction, has also been verified through various indicators of datasets.

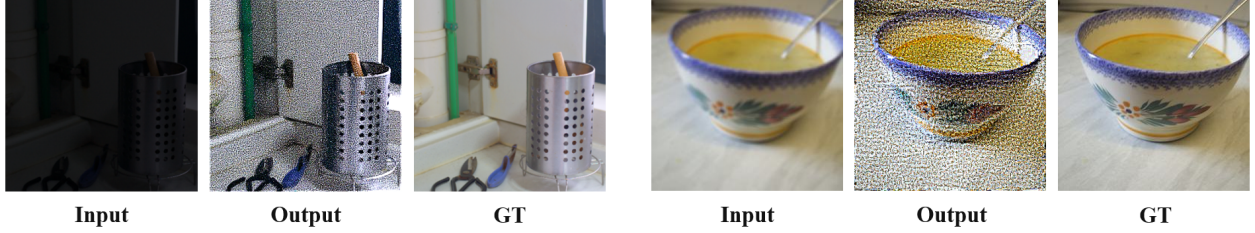


Figure 10: Qualitative results when the fixed guidance scale is biased towards a larger value of $s = 80000$.

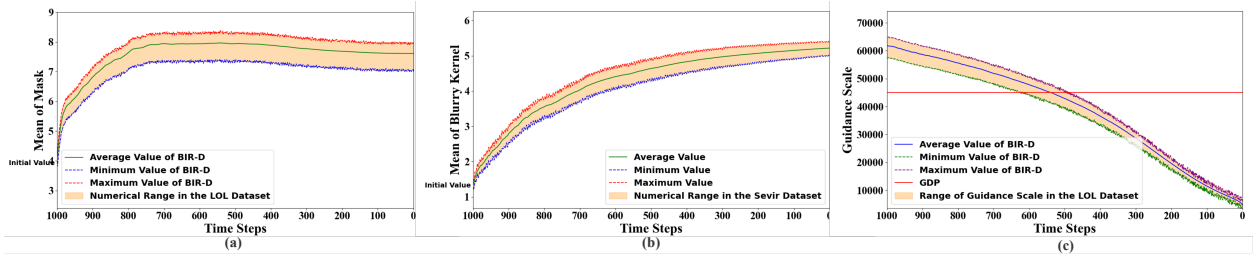


Figure 11: Illustration of (a) the variation of the mean of optimizable convolutional kernel parameters in each step of the sampling process. (b) The variation of the mean of degradation mask in each step of the sampling process. (c) The variation of adaptive guidance scale in each step of the sampling process. These experiments are performed on LOL dataset.

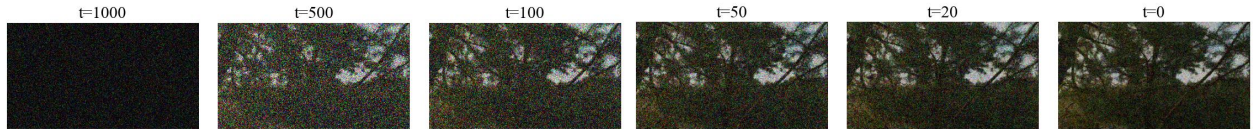


Figure 12: The changing of degradation mask during the sampling process in HDR recovery.

Acknowledgment

The authors would like to thank Zhaoyang Lyu for his technical assistance.

References

- [1] Tao Yang, Peiran Ren, Xuansong Xie, and Lei Zhang. Gan prior embedded network for blind face restoration in the wild. In *Proceedings of the IEEE/CVF conference on computer vision and pattern recognition*, pages 672–681, 2021.
- [2] SG Gino Sophia, Syed Umar, and N Visvas. An efficient method for blind image restoration using gan. In *2022 international conference on innovative computing, intelligent communication and smart electrical systems (ICSSES)*, pages 1–8. IEEE, 2022.
- [3] Xu Deng, Hao Zhang, and Xiaojie Li. Hpg-gan: High-quality prior-guided blind face restoration generative adversarial network. *Electronics*, 12(16):3418, 2023.
- [4] Lin Luo, Jiaqi Bao, Jinlong Li, and Xiaorong Gao. Blind restoration of astronomical image based on deep attention generative adversarial neural network. *Optical Engineering*, 61(1):013101–013101, 2022.
- [5] Zhixin Wang, Ziyang Zhang, Xiaoyun Zhang, Huangjie Zheng, Mingyuan Zhou, Ya Zhang, and Yanfeng Wang. Dr2: Diffusion-based robust degradation remover for blind face restoration. In *Proceedings of the IEEE/CVF Conference on Computer Vision and Pattern Recognition*, pages 1704–1713, 2023.
- [6] Xunpeng Yi, Han Xu, Hao Zhang, Linfeng Tang, and Jiayi Ma. Diff-retinex: Rethinking low-light image enhancement with a generative diffusion model. In *Proceedings of the IEEE/CVF International Conference on Computer Vision*, pages 12302–12311, 2023.
- [7] Charles Laroche, Andrés Almansa, and Eva Coupete. Fast diffusion em: a diffusion model for blind inverse problems with application to deconvolution. In *Proceedings of the IEEE/CVF Winter Conference on Applications of Computer Vision*, pages 5271–5281, 2024.

- [8] Nan Wu, Guodong Wang, Hong Zhang, Guojia Hou, and Baoxiang Huang. Color blurred image restoration based on multichannel nonlinear diffusion model. In 2017 10th International Congress on Image and Signal Processing, BioMedical Engineering and Informatics (CISP-BMEI), pages 1–6. IEEE, 2017.
- [9] Yiman Zhu, Lu Wang, Jingyi Yuan, and Yu Guo. Diffusion model based low-light image enhancement for space satellite. arXiv preprint arXiv:2306.14227, 2023.
- [10] Ben Fei, Zhaoyang Lyu, Liang Pan, Junzhe Zhang, Weidong Yang, Tianyue Luo, Bo Zhang, and Bo Dai. Generative diffusion prior for unified image restoration and enhancement. In Proceedings of the IEEE/CVF Conference on Computer Vision and Pattern Recognition, pages 9935–9946, 2023.
- [11] Bahjat Kawar, Michael Elad, Stefano Ermon, and Jiaming Song. Denoising diffusion restoration models. Advances in Neural Information Processing Systems, 35:23593–23606, 2022.
- [12] Yinhuai Wang, Jiwen Yu, Runyi Yu, and Jian Zhang. Unlimited-size diffusion restoration. In Proceedings of the IEEE/CVF Conference on Computer Vision and Pattern Recognition, pages 1160–1167, 2023.
- [13] Prafulla Dhariwal and Alexander Nichol. Diffusion models beat gans on image synthesis. Advances in neural information processing systems, 34:8780–8794, 2021.
- [14] Peiqing Yang, Shangchen Zhou, Qingyi Tao, and Chen Change Loy. Pgdif: Guiding diffusion models for versatile face restoration via partial guidance. Advances in Neural Information Processing Systems, 36, 2024.
- [15] Xinqi Lin, Jingwen He, Ziyang Chen, Zhaoyang Lyu, Ben Fei, Bo Dai, Wanli Ouyang, Yu Qiao, and Chao Dong. Diffbir: Towards blind image restoration with generative diffusion prior. arXiv preprint arXiv:2308.15070, 2023.
- [16] Bahjat Kawar, Jiaming Song, Stefano Ermon, and Michael Elad. Jpeg artifact correction using denoising diffusion restoration models. In Neural Information Processing Systems (NeurIPS) Workshop on Score-Based Methods, 2022.
- [17] Ozan Özdenizci and Robert Legenstein. Restoring vision in adverse weather conditions with patch-based denoising diffusion models. IEEE Transactions on Pattern Analysis and Machine Intelligence, 2023.
- [18] Ziwei Luo, Fredrik K Gustafsson, Zheng Zhao, Jens Sjölund, and Thomas B Schön. Refusion: Enabling large-size realistic image restoration with latent-space diffusion models. In Proceedings of the IEEE/CVF conference on computer vision and pattern recognition, pages 1680–1691, 2023.
- [19] Ruxin Wang and Dacheng Tao. Training very deep cnns for general non-blind deconvolution. IEEE Transactions on Image Processing, 27(6):2897–2910, 2018.
- [20] M Anand, A Ashwin Natraj, V Jeya Maria Jose, K Subramanian, Priyanka Bhardwaj, R Pandeewari, and S Deivalakshmi. Tackling multiple visual artifacts: Blind image restoration using conditional adversarial networks. In Computer Vision and Image Processing: 4th International Conference, CVIP 2019, Jaipur, India, September 27–29, 2019, Revised Selected Papers, Part II 4, pages 331–342. Springer, 2020.
- [21] Hyungjin Chung, Jeongsol Kim, Sehui Kim, and Jong Chul Ye. Parallel diffusion models of operator and image for blind inverse problems. In Proceedings of the IEEE/CVF Conference on Computer Vision and Pattern Recognition, pages 6059–6069, 2023.
- [22] Vaishnav Potlapalli, Syed Waqas Zamir, Salman Khan, and Fahad Shahbaz Khan. Promptir: Prompting for all-in-one blind image restoration. arXiv preprint arXiv:2306.13090, 2023.
- [23] Jonathan Ho, Ajay Jain, and Pieter Abbeel. Denoising diffusion probabilistic models. Advances in neural information processing systems, 33:6840–6851, 2020.
- [24] Alexander Quinn Nichol and Prafulla Dhariwal. Improved denoising diffusion probabilistic models. In International conference on machine learning, pages 8162–8171. PMLR, 2021.
- [25] Xintao Wang, Yu Li, Honglun Zhang, and Ying Shan. Towards real-world blind face restoration with generative facial prior. In Proceedings of the IEEE/CVF conference on computer vision and pattern recognition, pages 9168–9178, 2021.
- [26] Shangchen Zhou, Kelvin Chan, Chongyi Li, and Chen Change Loy. Towards robust blind face restoration with codebook lookup transformer. Advances in Neural Information Processing Systems, 35:30599–30611, 2022.
- [27] Xingang Pan, Xiaohang Zhan, Bo Dai, Dahua Lin, Chen Change Loy, and Ping Luo. Exploiting deep generative prior for versatile image restoration and manipulation. IEEE Transactions on Pattern Analysis and Machine Intelligence, 44(11):7474–7489, 2021.
- [28] Yaniv Romano, Michael Elad, and Peyman Milanfar. The little engine that could: Regularization by denoising (red). SIAM Journal on Imaging Sciences, 10(4):1804–1844, 2017.

- [29] Bahjat Kawar, Gregory Vaksman, and Michael Elad. Snips: Solving noisy inverse problems stochastically. *Advances in Neural Information Processing Systems*, 34:21757–21769, 2021.
- [30] Yinhuai Wang, Jiwen Yu, and Jian Zhang. Zero-shot image restoration using denoising diffusion null-space model. *arXiv preprint arXiv:2212.00490*, 2022.
- [31] C Wei, W Wang, W Yang, and J Liu. Deep retinex decomposition for low-light enhancement. *arxiv* 2018. *arXiv preprint arXiv:1808.04560*, 1808.
- [32] Jiaying Liu, Dejia Xu, Wenhan Yang, Minhao Fan, and Haofeng Huang. Benchmarking low-light image enhancement and beyond. *International Journal of Computer Vision*, 129:1153–1184, 2021.
- [33] Chongyi Li, Chunle Guo, Linghao Han, Jun Jiang, Ming-Ming Cheng, Jinwei Gu, and Chen Change Loy. Low-light image and video enhancement using deep learning: A survey. *IEEE Transactions on Pattern Analysis and Machine Intelligence*, 44(12):9396–9416, 2021.
- [34] Lin Zhang, Lijun Zhang, Xiao Liu, Ying Shen, Shaoming Zhang, and Shengjie Zhao. Zero-shot restoration of back-lit images using deep internal learning. In *Proceedings of the 27th ACM International Conference on Multimedia*, pages 1623–1631, 2019.
- [35] Chunle Guo, Chongyi Li, Jichang Guo, Chen Change Loy, Junhui Hou, Sam Kwong, and Runmin Cong. Zero-reference deep curve estimation for low-light image enhancement. In *Proceedings of the IEEE/CVF Conference on Computer Vision and Pattern Recognition*, pages 1780–1789, 2020.
- [36] Chongyi Li, Chunle Guo, and Chen Change Loy. Learning to enhance low-light image via zero-reference deep curve estimation. *IEEE Transactions on Pattern Analysis and Machine Intelligence*, 44(8):4225–4238, 2021.
- [37] Anqi Zhu, Lin Zhang, Ying Shen, Yong Ma, Shengjie Zhao, and Yicong Zhou. Zero-shot restoration of underexposed images via robust retinex decomposition. In *2020 IEEE International Conference on Multimedia and Expo (ICME)*, pages 1–6. IEEE, 2020.
- [38] Eduardo Pérez-Pellitero, Sibi Catley-Chandar, Ales Leonardis, and Radu Timofte. Ntire 2021 challenge on high dynamic range imaging: Dataset, methods and results. In *Proceedings of the IEEE/CVF Conference on Computer Vision and Pattern Recognition*, pages 691–700, 2021.
- [39] Seungjun Nah, Tae Hyun Kim, and Kyoung Mu Lee. Deep multi-scale convolutional neural network for dynamic scene deblurring. In *Proceedings of the IEEE conference on computer vision and pattern recognition*, pages 3883–3891, 2017.
- [40] Ziyi Shen, Wenguan Wang, Xiankai Lu, Jianbing Shen, Haibin Ling, Tingfa Xu, and Ling Shao. Human-aware motion deblurring. In *Proceedings of the IEEE/CVF International Conference on Computer Vision*, pages 5572–5581, 2019.
- [41] Xintian Mao, Yiming Liu, Fengze Liu, Qingli Li, Wei Shen, and Yan Wang. Intriguing findings of frequency selection for image deblurring. In *Proceedings of the AAAI Conference on Artificial Intelligence*, volume 37, pages 1905–1913, 2023.
- [42] Shangzhe Wu, Jiarui Xu, Yu-Wing Tai, and Chi-Keung Tang. Deep high dynamic range imaging with large foreground motions. In *Proceedings of the European Conference on Computer Vision (ECCV)*, pages 117–132, 2018.
- [43] Dasong Li, Yi Zhang, Ka Chun Cheung, Xiaogang Wang, Hongwei Qin, and Hongsheng Li. Learning degradation representations for image deblurring. In *European Conference on Computer Vision*, pages 736–753. Springer, 2022.
- [44] Qingsen Yan, Dong Gong, Qinfeng Shi, Anton van den Hengel, Chunhua Shen, Ian Reid, and Yanning Zhang. Attention-guided network for ghost-free high dynamic range imaging. In *Proceedings of the IEEE/CVF Conference on Computer Vision and Pattern Recognition*, pages 1751–1760, 2019.
- [45] Liangyu Chen, Xiaojie Chu, Xiangyu Zhang, and Jian Sun. Simple baselines for image restoration. In *European conference on computer vision*, pages 17–33. Springer, 2022.
- [46] Yuzhen Niu, Jianbin Wu, Wenxi Liu, Wenzhong Guo, and Rynson WH Lau. Hdr-gan: Hdr image reconstruction from multi-exposed ldr images with large motions. *IEEE Transactions on Image Processing*, 30:3885–3896, 2021.
- [47] Zhenxuan Fang, Fangfang Wu, Weisheng Dong, Xin Li, Jinjian Wu, and Guangming Shi. Self-supervised non-uniform kernel estimation with flow-based motion prior for blind image deblurring. In *Proceedings of the IEEE/CVF conference on computer vision and pattern recognition*, pages 18105–18114, 2023.
- [48] Georgios Batzolis, Jan Stanczuk, Carola-Bibiane Schönlieb, and Christian Etmann. Conditional image generation with score-based diffusion models. *arXiv preprint arXiv:2111.13606*, 2021.

-
- [49] Shuhang Wang, Jin Zheng, Hai-Miao Hu, and Bo Li. Naturalness preserved enhancement algorithm for non-uniform illumination images. IEEE transactions on image processing, 22(9):3538–3548, 2013.
- [50] Anish Mittal, Rajiv Soundararajan, and Alan C Bovik. Making a “completely blind” image quality analyzer. IEEE Signal processing letters, 20(3):209–212, 2012.